Supporting Information

A multi-dimensional and level-by-level assembly strategy for constructing flexible and sandwich-type nanoheterostructures for high-performance electromagnetic interference shielding

Caichao Wan,*[a] Yue Jiao,[b] Xianjun Li,[a] Wenyan Tian,[a] Jian Li,[b] Yiqiang Wu*[a]

[a]College of Materials Science and Engineering, Central South University of Forestry and Technology, Changsha 410004, PR China. E-mails: wancaichaojy@163.com (C. W.), wuyq0506@126.com (Y. W.).

[b]Material Science and Engineering College, Northeast Forestry University, Harbin 150040, PR China.

Outlines

1. SEM image of cotton cloth

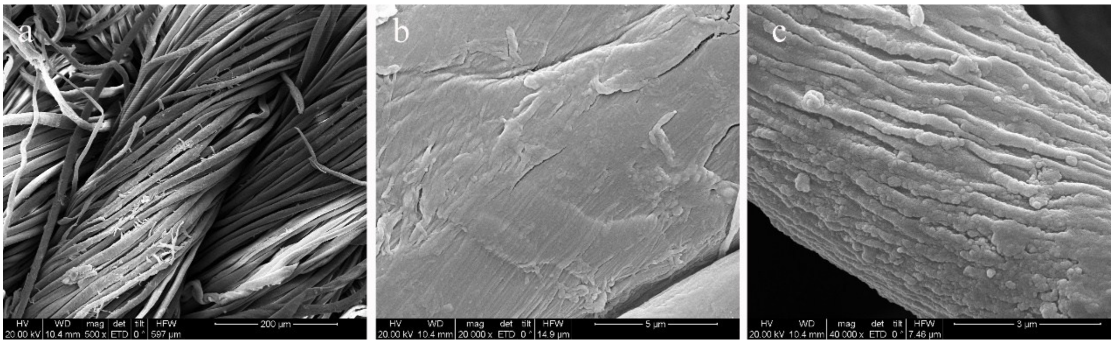

Figure S1. SEM images of the cotton cloth (a, b) and CFs (c).

By comparing Fig. S1a-b and 1c, we can find that the pyrolysis decreases the fiber diameter and transforms the smooth surface of cotton fibers to the rough surface of CFs.

2. Mechanism of depositing Ni NPs onto CFs by magnetron sputtering

For the magnetron sputtering process (Fig. S2), inert gas atoms (Ar) were ionized and accelerated owing to the potential difference between the negatively biased target (cathode) and the anode, and the interaction of ions with the target (namely metallic Ni) surface caused the ejection (sputtering) of Ni atoms which condensed on the surface of CFs.[S1, S2] Primary merits of magnetron sputtering can be summarized as follows: (1) high deposition rates, (2) ease of sputtering any metals or alloys, (3) high-purity films, (4) high adhesion of films, (5) excellent coverage of steps and small features, (6) ability to coat heat-sensitive substrates, (7) ease of automation and (8) excellent uniformity on large-area substrates.[S3-S6]

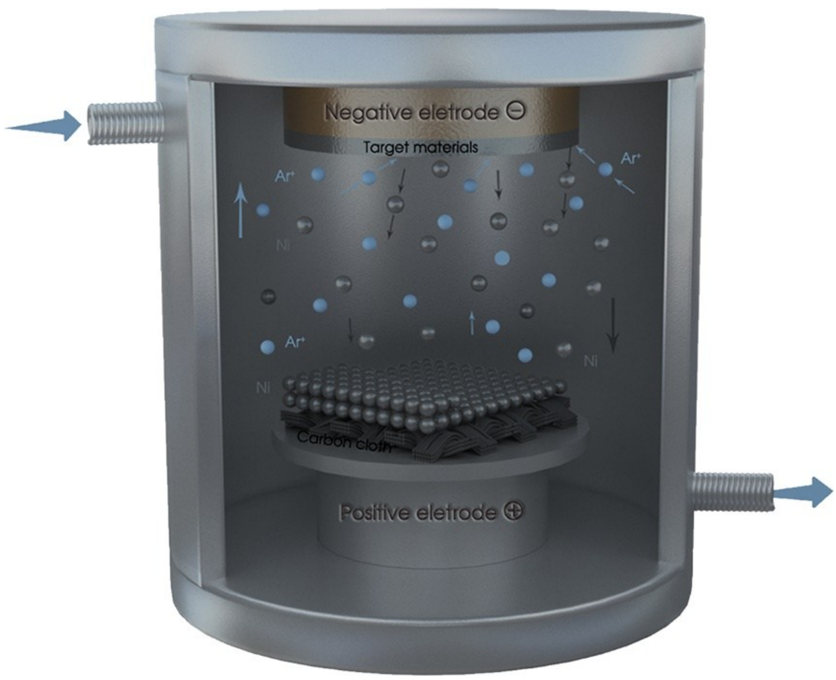

Figure S2. Schematic illustration of the magnetron sputtering of metallic Ni on the surface of CFs.

3. Mechanism of growing DLG onto Ni NPs/CFs by PECVD

For the PEVCD (Figure S3), the growth mechanism of DLG on the Ni NPs/CFs can be briefly described as follows: firstly, the trace amount of CH_4 is introduced into the PECVD chamber and produces high concentration of carbon reactive radicals within a short time due to the assistance of plasma;[S7] secondly, during the PECVD of graphene, the hydrocarbon is decomposed and carbon atoms from the decomposed CH_4 gas absorb on the surface of the Ni layer, leading to the growth of 2D graphene films;[S8] thirdly, the layer growth turns into vertical growth due to the strain energy in the edges and defects of initial graphene (the intermediate layer may not be able to continue to form bulk crystal and thus causes a transition from 2D complete films to 3D clusters).[S8-S10] Besides, the plasma can ensure the 3D growth of vertical graphene nanosheets, since reactive carbon radicals generated in the plasma would reach the edge frequently and thus diffuse outward.

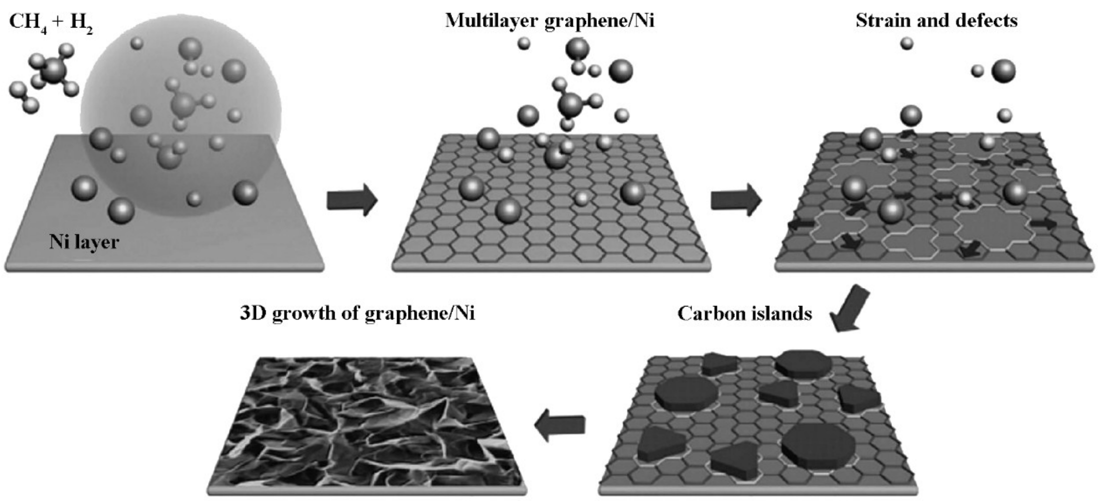

Figure S3. Schematic illustration of the 3D growth process of graphene on nickel substrate in a PECVD system: (I) breakage of carbon–hydrogen bonds; (II) formation of multilayer graphene on a Ni surface; (III) strain and defects on 2D graphene film after a period of growth; (IV) transition from 2D to 3D growth due to accumulated strain and defects; (V) development of 3D graphene clusters on a Ni substrate due to the high mobility of carbon atoms and van der Waals force between neighboring graphene sheets. Reproduced with permission [S7].

4. XRD pattern of cotton cloth

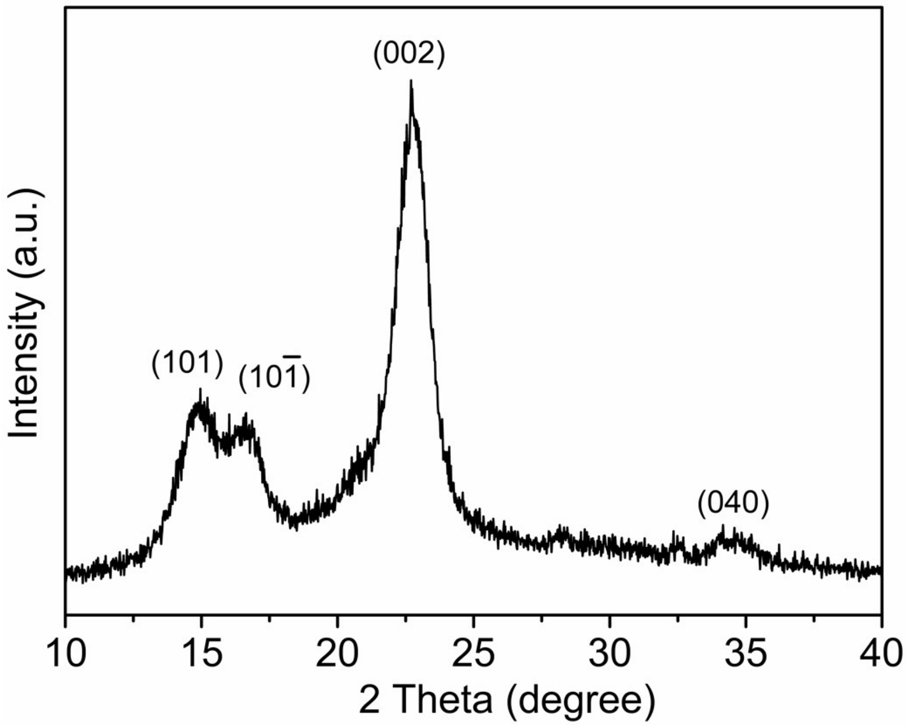

Figure S4. XRD pattern of the cotton cloth.

The XRD pattern of the cotton cloth (the precursor of CFs) is shown in Fig. S4. The cotton cloth exhibits peaks at around 15.0°, 16.6°, 22.7° and 34.7°, corresponding to the (101), (10$\bar{1}$), (002) and (040) planes of cellulose I crystal structure.[S11]

5. Calculation method of BET surface area of graphene in DLG/Ni NPs/CFs

The BET surface areas of Ni NPs/CFs and DLG/Ni NPs/CFs are 12.9 $m^2 g^{-1}$ and 16.8 $m^2 g^{-1}$, respectively. Besides, their areal densities are 7.16 mg cm^{-2} and 7.34 mg cm^{-2}, respectively. The weight was accurately measured by microbalance (MS105DU, Mettler Toledo) with an accuracy of 0.01 mg. Therefore, the specific surface area of the graphene composition in DLG/Ni NPs/CFs can be roughly calculated to be $(16.8–12.9)/[(7.34–7.16)/7.34)] \approx 159$ $m^2 g^{-1}$.

6. Determination of skin depth and its variation with frequency

The skin depth δ is the distance up to which the intensity of the electromagnetic wave decreases to 1/e of its original strength. The δ is related to the angular frequency ω, relative permeability μ and frequency dependent conductivity σ_{AC} by the equation, $\delta=\sqrt{2/\sigma_{AC}\omega\mu}$ ($\omega=2\pi f$, $\mu=\mu_0\mu_r$, $\mu_0=4\pi\times10^{-7}$ H m^{-1}, $\sigma_{AC}=2\pi f\varepsilon_0\varepsilon''$, $\varepsilon_0\approx8.85\times10^{-12}$ F m^{-1}, ε'' is the imaginary part of complex permittivity ε_r, μ_r is the complex permeability).[S12] The plot of δ versus frequency in the range of 8.2–12.4 GHz is presented in Fig. S5. The skin depth δ for DLG/Ni NPs/CFs is calculated to be 0.55–0.62 mm, meaning that this composite should have a thickness greater than this range.

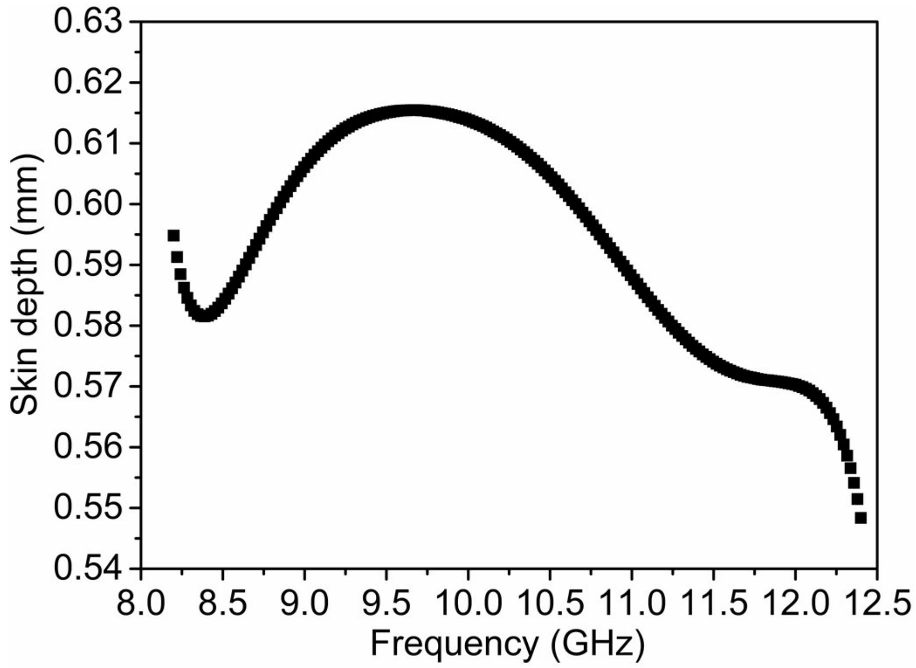

Figure S5. Skin depth δ of DLG/Ni NPs/CFs versus frequency in the range of 8.2–12.4 GHz (X-band).

7. Schematic of EMI shielding mechanism and calculation formulas of SE_{total}, SE_A and SE_R

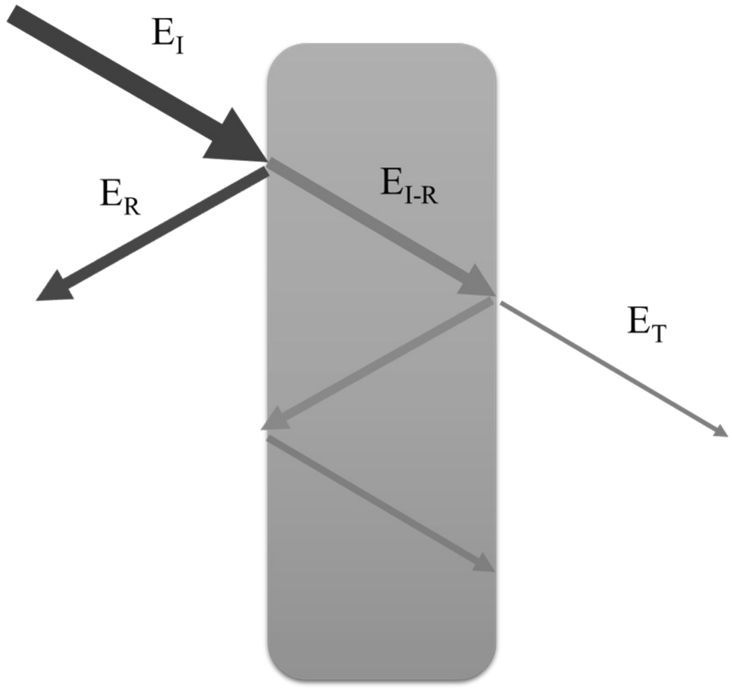

Figure S6. Schematic diagram of EMI shielding mechanism in an electrical conductor.

When an electromagnetic plane wave (E_I) strikes a monolithic conductive material, two waves will be created at the external surface, namely a reflected wave (E_R) and a transmitted wave ($E_{I\text{–}R}$), as shown in Fig. S6. As the transmitted wave from the external surface ($E_{I\text{–}R}$) travels in the conductive shield, the strength of the wave exponentially decreases due to absorption (multiple reflections). The absorbed energy is dissipated as heat. Once the wave reaches the second surface of the shield, a portion of the wave will pass through the surface (E_T) and a portion will be reflected into the first surface.[S13]

EMI shielding property is evaluated by shielding effectiveness expressed in decibels (dB) over the frequency range of 8.2–12.4 GHz (X-band). A higher decibel level reveals less energy transmitted through shielding materials. The total shielding effectiveness (SE_{total}) can be expressed as:[S14]

$$SE_{total}(\mathrm{dB}) = 10\log\frac{P_i}{P_t} = SE_A + SE_R + SE_M \tag{1}$$

where P_i and P_t are the incident and transmitted electromagnetic power, respectively. SE_R and SE_A are the shielding effectiveness from reflection and absorption, respectively. SE_M is multiple reflection effectiveness inside the material, which can be negligible when SE_{total} > 15 dB. Besides, SE_R and SE_A can be described as:[S15]

$$SE_R = -10\log(1-R) \tag{2}$$

$$SE_A = -10\log\left[T/(1-R)\right] \tag{3}$$

where R and T are reflected power and transmitted power, respectively. R and T are calculated based on the S-parameters obtained from the vector network analyzer as follows: $R = |S_{11}|^2 = |S_{22}|^2$ and $T = |S_{12}|^2 = |S_{21}|^2$,[S16] respectively.

8. SE_{total}, SE_A and SE_R values of cotton fibers

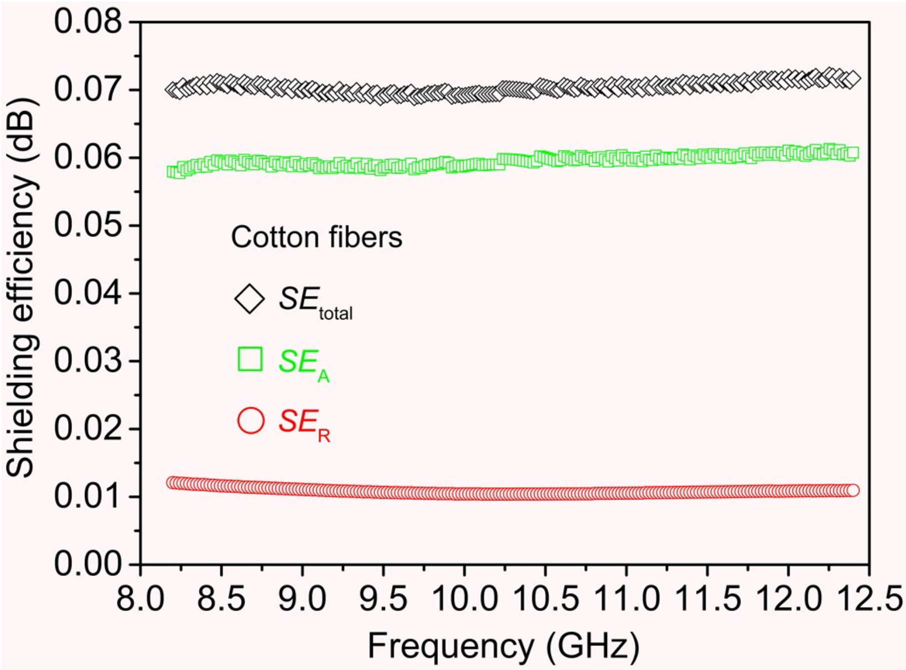

Figure S7. SE_{total}, SE_A and SE_R values of the cotton fibers.

The low SE_{total} of 0.07 dB is attributed to its ignorable magnetic permeability and electrical conductivity which are both decisive for EMI shielding.[S17]

9. Classification of electromagnetic shielding textiles

Table S1. Classification of electromagnetic shielding textiles.[S18, S19]

Type	Grade	*SE*[I] (dB)	Classification	*ES*[II] (%)
Class I Professional use[III]	AAAAA	$SE > 60$	Excellent	$ES > 99.9999\%$
	AAAA	$60 \geq SE > 50$	Very good	$99.9999\% \geq ES > 99.999\%$
	AAA	$50 \geq SE > 40$	good	$99.999\% \geq ES > 99.99\%$
	AA	$40 \geq SE > 30$	Moderate	$99.99\% \geq ES > 99.9\%$
	A	$30 \geq SE > 20$	Fair	$99.9\% \geq ES > 99.0\%$
Class II General use[IV]	AAAAA	$SE > 30$	Excellent	$ES > 99.9\%$
	AAAA	$30 \geq SE > 20$	Very good	$99.9\% \geq ES > 99.0\%$
	AAA	$20 \geq SE > 10$	good	$99.0\% \geq ES > 90.0\%$
	AA	$10 \geq SE > 7$	Moderate	$90\% \geq ES > 80\%$
	A	$7 \geq SE > 5$	Fair	$80\% \geq ES > 70\%$

[I]: *SE* = Shielding Effectiveness (dB); [II]: *ES* = Percentage of Electromagnetic Shielding (%); [III]: medical equipment, quarantine material, professional security uniform for electronic manufacturer, electronic kit, or other new applications; [IV]: casual wear, office uniform, maternity dress, apron, consumptive electronic products, and communication related products, or other new applications.

10. ε', ε'', μ' and μ'' values of DLG/Ni NPs/CFs in the range of X-band

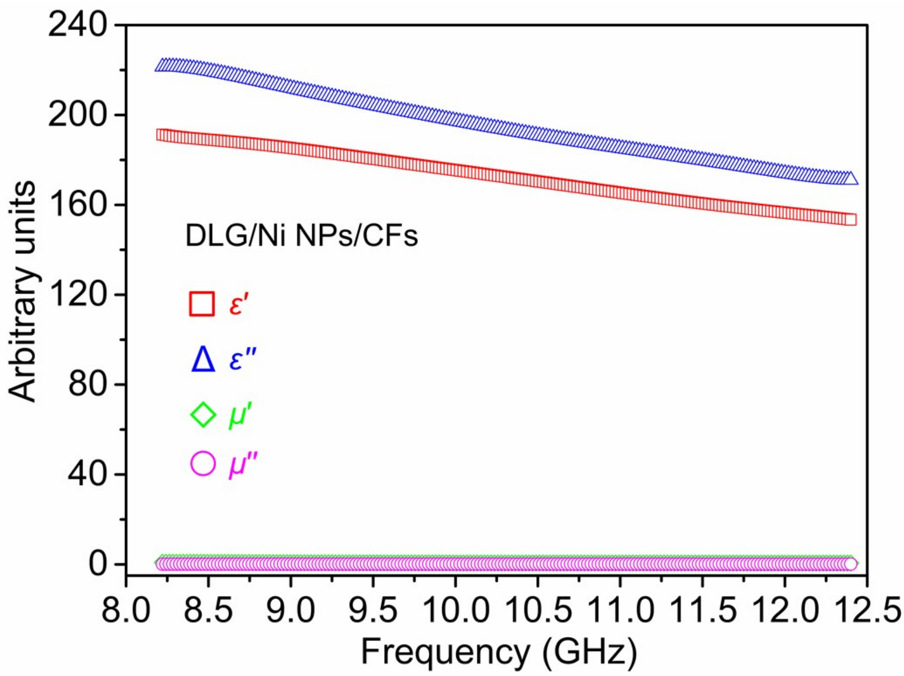

Figure S8. ε', ε'', μ' and μ'' values of DLG/Ni NPs/CFs in the range of X-band (8.2–12.4 GHz).

References

[S1] P. J. Kelly, R. D. Arnell, *Vacuum* **2000**, 56, 159.

[S2] C. Wan, Y. Jiao, J. Li, *Journal of Materials Chemistry A* **2017**, 5, 17267.

[S3] I. Safi, *Surface and Coatings Technology* **2000**, 127, 203.

[S4] M. J. Lee, S. I. Kim, C. B. Lee, H. Yin, S. E. Ahn, B. S. Kang, K. H. Kim, J. C. Park, C. J. Kim, I. Song, *Advanced Functional Materials* **2009**, 19, 1587.

[S5] X. Hou, H. Zhang, L. Jiang, *Angewandte Chemie International Edition* **2012**, 51, 5296.

[S6] J. Wang, X. Jiang, L. Zhang, Z. Qiao, B. Gao, G. Yang, H. Huang, *Nano Energy* **2015**, 12, 597.

[S7] M. Li, D. Liu, D. Wei, X. Song, D. Wei, A. T. S. Wee, *Advanced Science* **2016**, 3, 1600003.

[S8] L. Jiang, T. Yang, F. Liu, J. Dong, Z. Yao, C. Shen, S. Deng, N. Xu, Y. Liu, H. J. Gao, *Advanced Materials* **2013**, 25, 250.

[S9] Y. Ma, H. Jang, S. J. Kim, C. Pang, H. Chae, *Nanoscale Research Letters* **2015**, 10, 308.

[S10] Z. Zhang, M. G. Lagally, *Science* **1997**, 276, 377.

[S11] X. P. Hu, Y. L. Hsieh, *Journal of Polymer Science Part B: Polymer Physics* **1996**, 34, 1451.

[S12] A. P. Singh, M. Mishra, D. P. Hashim, T. N. Narayanan, M. G. Hahm, P. Kumar, J. Dwivedi, G. Kedawat, A. Gupta, B. P. Singh, A. Chandra, R. Vajtai, S. K. Dhawan, P. M. Ajayan, B. K. Gupta, *Carbon* **2015**, 85, 79.

[S13] M. H. Al-Saleh, U. Sundararaj, *Carbon* **2009**, 47, 1738.

[S14] J. Dalal, S. Lather, A. Gupta, S. Dahiya, A. Maan, K. Singh, S. Dhawan, A. Ohlan, *Composites Science and Technology* **2018**, 165, 222.

[S15] S. Kumar, G. Datt, A. Santhosh Kumar, A. Abhyankar, *Journal of Applied Physics* **2016**, 120, 164901.

[S16] H. Mei, D. Han, S. Xiao, T. Ji, J. Tang, L. Cheng, *Carbon* **2016**, 109, 149.

[S17] H. Kim, K. Kim, C. Lee, J. Joo, S. Cho, H. Yoon, D. Pejaković, J.-W. Yoo, A. Epstein, *Applied Physics Letters* **2004**, 84, 589.

[S18] H. Zhao, L. Hou, S. Bi, Y. Lu, *ACS Applied Materials & Interfaces* **2017**, 9, 33059.

[S19] FTTS-FA-003 (test method of specified requirements of electromagnetic shielding textiles), *Committee for conformity assessment on accreditation and certification of functional and technical textiles* **2003**, 1.